

NJC

Accepted Manuscript



This is an *Accepted Manuscript*, which has been through the Royal Society of Chemistry peer review process and has been accepted for publication.

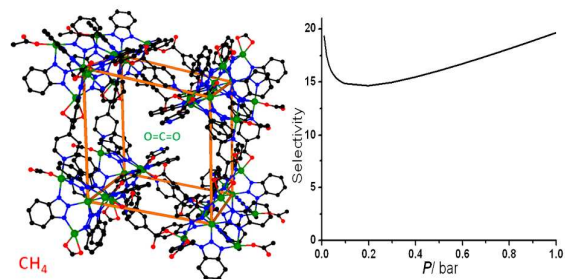
Accepted Manuscripts are published online shortly after acceptance, before technical editing, formatting and proof reading. Using this free service, authors can make their results available to the community, in citable form, before we publish the edited article. We will replace this *Accepted Manuscript* with the edited and formatted *Advance Article* as soon as it is available.

You can find more information about *Accepted Manuscripts* in the [Information for Authors](#).

Please note that technical editing may introduce minor changes to the text and/or graphics, which may alter content. The journal's standard [Terms & Conditions](#) and the [Ethical guidelines](#) still apply. In no event shall the Royal Society of Chemistry be held responsible for any errors or omissions in this *Accepted Manuscript* or any consequences arising from the use of any information it contains.



www.rsc.org/njc



Porous layer built from connecting of orthorhombic cages with accessible metal centers shows high selectivity for CO₂ over CH₄.

Cite this: DOI: 10.1039/c0xx00000x

www.rsc.org/xxxxxx

ARTICLE TYPE

Microporous Metal-Organic Layer Built from Pentanuclear Tetrahedral Units: Gas Sorption and Magnetism

Yan-Xi Tan^{a,b}, Ying Zhang^{*a}, Yan-Ping He^{*b}, and Yan-Jun Zheng^{*a}

Received (in XXX, XXX) Xth XXXXXXXXXX 200X, Accepted Xth XXXXXXXXXX 200X

DOI: 10.1039/b000000x

Presented here is a porous layer motif **1** built from pentanuclear tetrahedral Ni-clusters with accessible metal centers. Activated **1** exhibits a high selectivity of 19.8 under 273 K and 1 bar for the separation of CO₂ over CH₄. Magnetic measurement shows the overall antiferromagnetic coupling between Ni(II) ions for **1**.

Metal-organic frameworks (MOFs) as a class of new porous materials with fascinating architectures and desirable topologies are widely applied especially in the areas of gas sorption/separation, heterogeneous catalysis and magnetism because of their diversified building units, large surface area and modifiable hole-wall.¹ Among these functionalities, the capture of CO₂ and H₂ is one of the most important aspects. One promising point for MOF adsorbent with strong affinity for binding CO₂ and H₂ is the presence of active metal centers in the pores.² For example, the high H₂ and CO₂ capacities of the well-known HKUST-1 and MOF-74 was due to the well defined accessible active metal centers exposed to the inner surface.³ To give birth to accessible active metal centers, one of the most effective approach is to construct secondary building blocks (SBUs) with potential unsaturated coordination sites, typically like the paddle-wheel Cu₂(COO)₄(H₂O)₂ unit, whose terminal solvent molecules can be removed by using thermal treatment or other methods.⁴

Compared to these simple metallic-carboxylic SBUs, the tetrahedral units with polynuclear metal remain rarely known in the formation of MOFs with promising gas separation properties. As a tetrahedral cluster with accessible active metal centers, [M₅(btz)₆(NO₃)₄(H₂O)₂], has been proven to construct porous cluster-based MOFs through the substitution reaction of NO₃⁻.⁵ For example, via a step-by-step assembly strategy, Tao and coworkers assembled two pentanuclear clusters {[Co₅(btz)₆(NO₃)₄(H₂O)₂} and [Ni₅(btz)₆(NO₃)₄(H₂O)₂] synthesized as SBUs with TCNQ (7,7,8,8-tetracyano-*p*-quinodimethane) to construct 3D diamond-like networks by taking advantage of substitutable sites NO₃⁻ in the tetrahedral clusters.^{5a} Subsequently, Wang's groups successfully produced three microporous interpenetrated frameworks by using a pre-designed tetrahedral metal cluster [Zn₅(btz)₆(NO₃)₄(H₂O)₂] and linear dicarboxylic acid.^{5b} As another kind of common organic ligands, pyridine carboxylate acids with different functional groups and different donor atoms, such as O and N atoms, have been used to build many MOFs.⁶ However, little experimental effort has focused on determining the MOFs based

on tetrahedral cluster and pyridine carboxylate ligands for effective gas sorption and separation.

After careful consideration, we chose benzotriazole (HBtz) and Ni(NO₃)₂·6H₂O to assemble an anticipated tetrahedral cluster [Ni₅(Btz)₆(H₂O)₂]⁴⁺ as a reaction precursor because similar pentanuclear clusters have proven to meet under the mixed dissolvent system of DMA and MeOH.^{5b} The unsaturated Ni centers of each tetrahedral clusters [Ni₅(Btz)₆(H₂O)₂]⁴⁺ are further coordinated by the pyridylic and carboxylic groups of isonicotinate (Ina) as well as acetic groups to form a two-dimensional (2D) pentanuclear nickel-based layer, namely Ni₅(Btz)₆(Ina)₃(NO₃)_{0.33}(CH₃COO)_{0.67}(DMA)(MeOH)_{0.67}·2DMA (**1**), which exhibits a novel 6-connected network possessing 1D channels with window size of about 5×12 Å² along *b* directions. Gas sorption measurements for the activated phase **1-hf** give a Langmuir surface area of 254.9 m²/g and a H₂ uptake of 101.5 cm³/g at 77 K and 1 bar as well as high selectivity (19.8) of CO₂

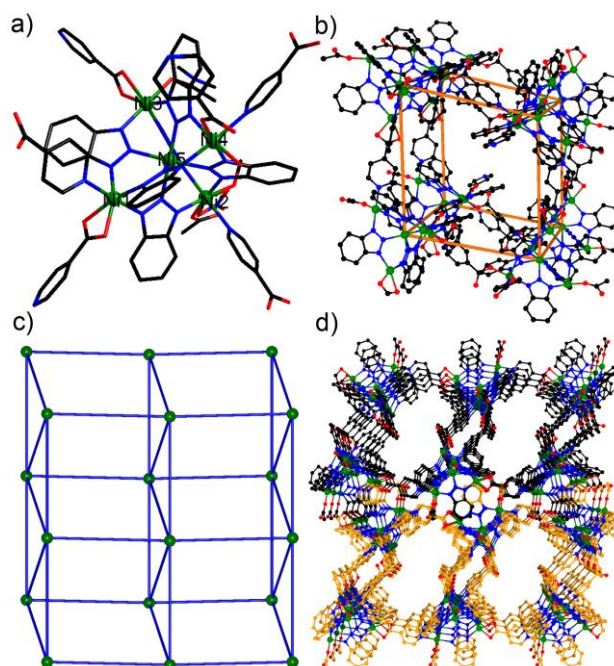


Figure 1. a) coordination environment of the Ni(II) centers in **1**; b) an orthorhombic cage composed of eight pentanuclear tetrahedral units; c) a novel 6-connected net with Schläfli symbol (3³·4¹⁰·5·6); d) the packing arrangement viewed along the *b* axis in compound **1**.

over CH₄ under 273 K and 1 bar. Magnetic measurement shows the overall antiferromagnetic coupling between Ni(II) ions for **1**.

The reaction of HBTz, HIna and Ni(NO₃)₂·6H₂O in a solution of DMA/MeOH (2:1, v/v) at 120 °C for 5 days afforded the blue crystals of **1**. Single-crystal X-ray diffraction analysis revealed that **1** crystallized in monoclinic space group *P*2₁/*c*. In the structure of **1** shown in Figure 1a, the anticipated pentanuclear cluster, which is composed of a tetrahedral arrangement of four six-coordinated Ni(II) ions centered on the fifth one, is similar to previous reported pentanuclear clusters also synthesized under the mixed solvent system of DMA and MeOH.⁵ Each of the six μ₃-Btz ligands straddles an edge of the tetrahedron and is bound to the central metal through the nitrogen atom in the 2-position. Six nitrogen atoms from six Btz ligands therefore complete the coordination sphere of the central Ni5 atom, while the remaining four Ni(II) atoms on the apical positions are all coordinated by three nitrogen atoms from three Btz ligands (Figure S1, ESI). The rest coordinated sites of Ni1, Ni2, Ni3, Ni4 are occupied by two oxygen atoms from a chelating carboxylate group of Ina ligand as well as one nitrogen atom from Ina ligand; two third of terminal MeOH molecule, one third of chelating NO₃⁻ group and one oxygen atoms from two third of carboxylate group of acetic acid derived from the decompose of DMA; two oxygen atoms from a chelating carboxylate group of Ina ligand as well as one terminal DMA molecule; one terminal H₂O molecule as well as one nitrogen atom from Ina ligand, respectively. Interestingly, as shown in Figure 1b, eight adjacent penta-nuclear [Ni₅(Btz)₆] clusters as SBUs are linked by Ina ligands to form an orthorhombic cage, leaving an irregular void with size of about 14.2×14.3 Å² (Ni5-to-Ni5 distance). Each such orthorhombic cage as super SBU further connects to other eight adjacent cages *via* sharing the penta-nuclear [Ni₅(Btz)₆] cluster as vertice along the *ac* plan, generating a porous layer motif Figure S2, ESI). In the structure of **1**, the acetate group and MeOH molecule as dangling ligands occupy two coordination sites of each Ni2 center, and then prevent the extension of framework in a direction to control the dimensionality of framework of **1** (Figure 1c). From the viewpoint of topology, the layer of **1** can be described as a novel 6-connected net with Schläfli symbol (3³.4¹⁰.5·6) by reducing each [Ni₅(Btz)₆] cluster as the 6-connected node (Figure 1c). There is weak C-H...O hydrogen-bond interaction between adjacent infinite layers (Figure S3, ESI), which further stack into a 3D supramolecular architecture in an ABAB fashion, leaving 1D channels with window size of about 5×12 Å² along *b* directions (Figure 1d). The solvent-accessible volume of **1** without all dissociative and terminal solvent molecules is approximately 3191.1 Å³ per unit cell (8145.8 Å³), being equal to about 39.2% of the total crystal volume estimated by PLATON. The dissociative and terminal solvent molecules in the free spaces are evidenced by thermal gravimetric analysis (TGA).

In order to examine the stability of the framework, TGA, X-ray powder diffraction (XRPD), and desolvation experiments were carried out. TGA curve of **1** reveals a weight loss of 20.80% at 120 °C, corresponding to the release of all terminal coordinating solvent ligands as well as two dissociative DMA molecules, one disorder MeOH and one disorder H₂O (Figure S4a, ESI) (calc. 20.2%). For gas adsorption studies, **1** was soaked at MeOH for one week and then dipped in CH₂Cl₂ for another week. It seems

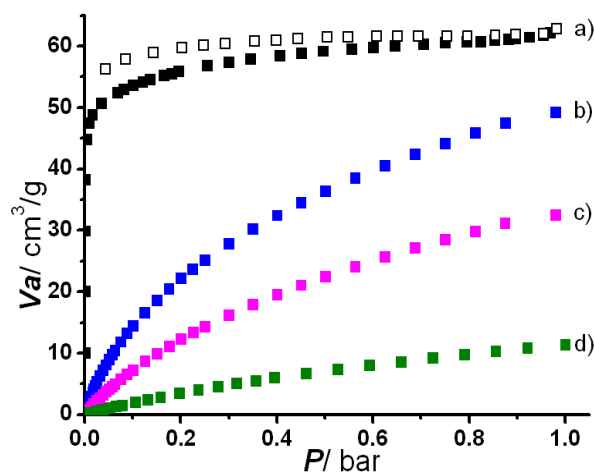


Figure 2. Gas sorption isotherms for **1-ht**: a) N₂ at 77 K; b) CO₂ at 273 K; c) CO₂ at 298 K; d) CH₄ at 273 K.

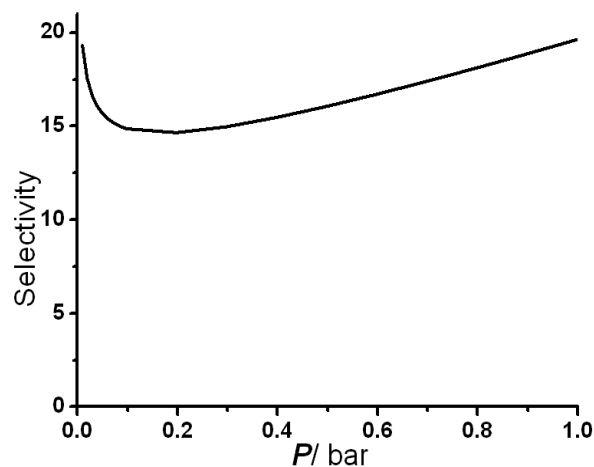


Figure 3. IAST predicted selectivity for CO₂/CH₄ at 273 K.

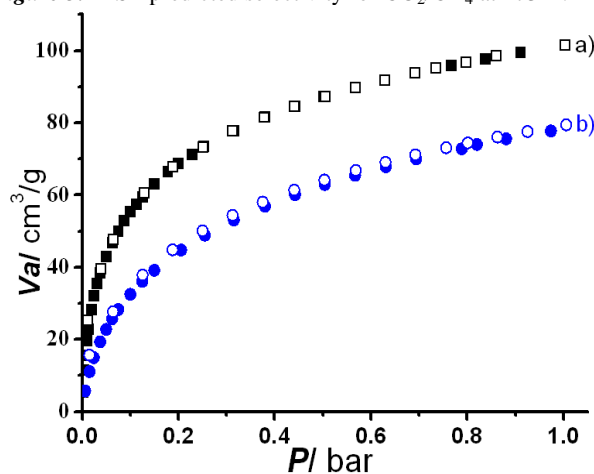


Figure 4. H₂ sorption isotherms at 77 (a) and 87 K (b) for **1-ht**.

that these dissociative and coordinative DMA molecules is easily replaced MeOH and CH₂Cl₂ during the solvent-exchange process (Figure S4b, ESI). by The CH₂Cl₂-exchanged sample was activated at 80 °C for 12 h under high vacuum to form the desolvated solid (**1-ht**). Further powder XRD experiments are carried out to verify the framework stability of **1-ht**. Compared to **1**, the PXRD patterns of **1-ht** have appeared obvious change

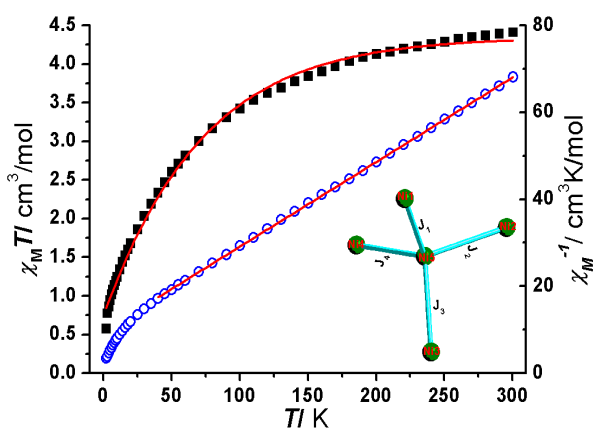


Figure 5. Temperature dependence of magnetic susceptibilities in the form of $\chi_M T$ at an applied field of 1000 Oe (red part for the least-square fitting at 2–300 K) and χ_M^{-1} vs. T plot (red part for the Curie–Weiss fitting) for **1**.

(Figure S5, ESI). It may be due to the slippage of layers after the removal of guest molecules.

The permanent porosity of **1-ht** was established by reversible gas sorption experiments using N_2 at 77 K, which shows a typical type I behavior characterized by a plateau reached at low relative pressure, indicating the presence of permanent micropores in **1-ht** (Figure 2a). The maximum N_2 uptake at 1 bar for **1-ht** is 62.9 cm^3/g , giving a BET and Langmuir surface areas of 180.5 and 254.9 m^2/g , respectively (Figure S6, ESI). Pore size distribution based on Horvath–Kawazoe (H–K) model gives a pore diameter of 7.6 Å (Figure S7, ESI). In the adsorption data of **1-ht**, a single data point at pressure of 0.98 bar gives a micropore volume of 0.097 cm^3/g , which is more less than the theoretical value of 0.357 cm^3/g calculated from crystallographic data because of the slippage of layers after activation.

The CO_2 uptake of **1-ht** at 273 and 298 K can reach 49.2 and 32.5 cm^3/g , respectively (Figure 2b and 2c). The enthalpies of CO_2 adsorption for **1-ht** were calculated by the virial equation from the adsorption isotherms measured at 273 and 298 K (Figure S8 and S10b, ESI). At zero coverage, the CO_2 isosteric heat of 28.1 kJ/mol for **1-ht** is comparable to those of MOFs with organic ammonium ions in the pores for strong CO_2 binding and indicates the strong interaction between CO_2 molecules and the host framework.²⁷ We speculate that such behavior is a result of the increased sorbate–sorbent interactions as the gas molecules access the pore region around the unsaturated metal sites. Although the CO_2 uptake ability for **1-ht** is at a moderate level compared to some currently reported MOFs, it shows high CO_2/CH_4 adsorption selectivity at ambient conditions. In contrast, CH_4 was hardly adsorbed by **1-ht** under the conditions of 273 K (just 10.8 cm^3/g) (Figure 2d). The experimental data are fits of the dual-site Langmuir–Freundlich mode (Figure S11, ESI) and the adsorption selectivity for equimolar mixture adsorption of CO_2 with respect to CH_4 are calculated using ideal solution adsorbed theory (IAST). The selectivity of CO_2 component with respect to CH_4 at 273 K is in excess of 14.5 for a range of pressures to 100 kPa (Figure 3). Notably, the high selective separation of CO_2/CH_4 suggests that **1-ht** may be a good candidate material for purification of natural gas.

Low-pressure H_2 adsorption isotherms collected for the sample of **1-ht** indicates that the framework has a strong affinity for

binding H_2 (Figure 4). At 77 K and 1.06 bar (800 Torr), it has a fully reversible H_2 uptake of 101.5 cm^3/g (0.91 wt%), a value surpassing that of the most favorable zeolite ZSM-5 (0.7 wt%)⁴⁵ and closing to those of recently reported MOFs.⁸ As a further test, a second H_2 adsorption isotherm was measured at 87 K, and two data sets were used to determine the isosteric heat of H_2 adsorption using the virial equation to understand the affinity of **1-ht** toward H_2 (Figure S9 and S10a, ESI), giving an isosteric heat of 7.2 kJ/mol under zero coverage.⁵⁰

The solid-state magnetic susceptibility of **1** was measured in the 2–300 K range at a field of 1000 Oe by using a SQUID magnetometer. The magnetic properties in the form of $\chi_M T$ vs. T plots are shown in Figure 5. At 300 K, the $\chi_M T$ value of **1** is 4.45 $cm^3 K mol^{-1}$, which is similar to the value that was previously reported for five uncoupled tetrahedral Ni-cluster.^{5a} However, it is smaller than that of three Ni5 clusters employing the 2-pyridylcyanoxime ligand because of the distinct magnetic-exchange pathway.⁹ As the temperature decreases, the value of $\chi_M T$ slowly decreases down to a minimum value of 0.58 $cm^3 K mol^{-1}$ for **1** at 2 K. The data in the range of 40–300 K obeys the Curie–Weiss law with $C = 5.14 cm^3 K mol^{-1}$, $\theta = -49.69$ K for **1**. The negative values of θ and the gradient of $\chi_M T$ vs. T plots should be due to the overall antiferromagnetic coupling between Ni(II) ions for **1**. The magnetic susceptibilities of **1** is fitted with a highly symmetric model to give $J_1 = -9.8$, $J_2 = -23.5$, $J_3 = -16.7$, $J_4 = -8.6$ and $g = 2.0$ for **1**. The large negative values of J further indicate that strong antiferromagnetic interaction exists among the Ni(II) centers.

In summary, by employing Ina ligands to assemble pentanuclear tetrahedral Ni-clusters, a new microporous layer **1** with exposed metal sites is successfully synthesized and features a porous layer motif with unusual 6-connected topology. Moreover, the desolvated solid **1-ht** not only exhibits a high H_2 uptake of 101.5 cm^3/g , but also separates CO_2 over CH_4 with selectivity of 19.8 under 273 K and 1 bar. Magnetic measurement shows the overall antiferromagnetic coupling between Ni(II) ions for **1**.

This work was supported by the grants from National Natural Science Foundation of China (U1162118); the Scientific Research Foundation of the Education Ministry for Returned Chinese Scholars.

Synthesis of $[Ni_5(Btz)_6(Ina)_3(H_2O)_2(CH_3COO)]_xG$ (1**).** HBtz (0.130 g, 1 mmol), HIna (0.062 g, 0.5 mmol), $Ni(NO_3)_2 \cdot 6H_2O$ (0.295 g, 1 mmol), 3 mL N,N-dimethylacetamide (DMA) and 1.5 mL methanol (MeOH) was sealed in a 20 mL vial and heated in an oven at 120 °C for 6 days. The vial was taken out and naturally cooled to room temperature. After washed with fresh methanol, blue block crystals were obtained in pure phase.

Notes and references

^a State Key Laboratory of Heavy Oil Processing, China University of Petroleum, Beijing, No.18 FuXue Road, ChangPing District, Beijing 102249, P.R. China. E-mail: tanyanxi2006@163.com; yingzh1977@163.com.

^b State Key Laboratory of Structural Chemistry, Fujian Institute of Research on the Structure of Matter, Chinese Academy of Sciences, Fuzhou, Fujian 350002, P. R. China.

Electronic Supplementary Information (ESI) available: [Experimental details, addition figures, TGA, powder X-ray patterns, adsorption isotherms and CIF file (CCDC-1022281)]. See DOI: 10.1039/b000000x/

- 1 (a) Y. Cui, Y. Yue, G. Qian, B. Chen, *Chem. Rev.*, 2012, **112**, 1126; (b)
J.-R. Li, J. Sculley and H.-C. Zhou, *Chem. Rev.*, 2012, **112**, 869; (c)
K. Sumida, D. L. Rogow, J. A. Mason, T. M. McDonald, E. D. Bloch,
Z. R. Herm, T.-H. Bae, J. R. Long, *Chem. Rev.*, 2012, **112**, 724; (d) A.
5 Dhakshinamoorthy, H. Garcia, *Chem. Soc. Rev.*, 2012, **41**, 5262; (e)
M. Kurmoo, *Chem. Soc. Rev.*, 2009, **38**, 1353; (f) D. Maspoch, D.
Ruiz-Molina, J. Veciana, *Chem. Soc. Rev.*, 2007, **36**, 770.
- 2 Y.-X. Tan, Y.-P. He, J. Zhang, *Chem. Commun.*, 2011, **47**, 10647.
- 3 (a) S. S. Kaye, J. R. Long, *J. Am. Chem. Soc.*, 2005, **127**, 6506; (b) J. L.
10 C. Rowsell, O. M. Yaghi, *J. Am. Chem. Soc.*, 2006, **128**, 1304; (c) X.
Kong, E. Scott, W. Ding, J. A. Mason, J. R. Long, J. A. Reimer, *J.
Am. Chem. Soc.*, 2012, **134**, 14341.
- 4 (a) Z. Wang, G. Chen and K. Ding, *Chem. Rev.*, 2009, **109**, 322; (b) A.
Henschel, K. Gedrich, R. Kraehnert, S. Kaskel, *Chem. Commun.*, 2008,
15 4192; (c) K. Schlichte, T. Kratzke, S. Kaskel, *Microporous
Mesoporous Mater.*, 2004, **73**, 81.
- 5 (a) Y.-L. Bai, J. Tao, R.-B. Huang, L.-S. Zheng, *Angew. Chem.*, 2008,
120, 5424; (b) X.-L. Wang, C. Qin, S.-X. Wu, K.-Z. Shao, Y.-Q. Lan,
S. Wang, D.-X. Zhu, Z.-M. Su, E.-B. Wang, *Angew. Chem. Int. Ed.*,
20 2009, **48**, 5291.
- 6 (a) Y.-P. He, Y.-X. Tan, J. Zhang, *CrystEngComm.*, 2012, **14**, 6359;
(b) Y.-X. Tan, Y.-P. He, Jian Zhang, *Chem. Mater.*, 2012, **24**, 4711.
- 7 J. An, N. L. Rosi, *J. Am. Chem. Soc.*, 2010, **132**, 5578.
- 8 (a) M. Higuchi, K. Nakamura, S. Horike, Y. Hijikata, N. Yanai, T.
25 Fukushima, J. Kim, K. Kato, M. Takata, D. Watanabe, S. Oshima, S.
Kitagawa, *Angew. Chem. Int. Ed.*, 2012, **124**, 8494; (b) Y. Q. Lan, S.
L. Li, H. L. Jiang, Q. Xu, *Chem. Eur. J.*, 2012, **18**, 8076.
- 9 J. Esteban, M. Font-Bardia, J. S. Costa, S. J. Teat, A. Escuer, *Inorg.
Chem.*, 2014, **53**, 3194.